Induced-Charge Enhancement of the Diffusion Potential in Membranes with Polarizable Nanopores

I. I. Ryzhkov,[1,2,*] D. V. Lebedev,[1] V. S. Solodovnichenko,[1] A. V. Shiverskiy,[1] and M. M. Simunin[2]
[1]Institute of Computational Modelling SB RAS, Federal Research Center KSC SB RAS, Akademgorodok 50, 660036 Krasnoyarsk, Russia
[2]Siberian Federal University, Svobodny 79, 660041 Krasnoyarsk, Russia
(Received 10 August 2017; published 29 November 2017)

When a charged membrane separates two salt solutions of different concentrations, a potential difference appears due to interfacial Donnan equilibrium and the diffusion junction. Here, we report a new mechanism for the generation of a membrane potential in polarizable conductive membranes via an induced surface charge. It results from an electric field generated by the diffusion of ions with different mobilities. For uncharged membranes, this effect strongly enhances the diffusion potential and makes it highly sensitive to the ion mobilities ratio, electrolyte concentration, and pore size. Theoretical predictions on the basis of the space-charge model extended to polarizable nanopores fully agree with experimental measurements in KCl and NaCl aqueous solutions.

DOI: 10.1103/PhysRevLett.119.226001

The understanding of ion transport in nanopores and nanochannels is of fundamental importance in various areas of science and technology, such as separation and purification [1], energy conversion [2], chemical sensors [3], and cell physiology [4]. Inspired by biological ion channels and pumps, researchers are working on the development of their synthetic analogues [5]. Tunable ion transport is realized by combining the pore design strategy (geometry and surface chemical modification) with external stimuli, such as the transmembrane potential, solution pH, temperature, light, etc. [6]. The ion transport through charged or uncharged membranes separating electrolytes with different concentrations has received much attention of researchers in various contexts including the design of nanofluidic devices [7], power generation from salinity gradients [8], potentiometric sensing [9], asymmetric diffusion transport [10], and osmotic flow generation [11].

A new class of membranes containing gold nanotubules that span a complete thickness of a porous polymeric support was suggested in Ref. [12]. It was shown that their selectivity can be reversible switched from anion to cation by changing the potential applied to the conductive membrane surface. Note that the transport of charged species through nanopores with polarizable walls can induce a surface charge and, thus, alter the pore transport characteristics. The induction of surface charge by an external electric field was employed in Ref. [13] for realizing nanopores with ion current rectification. The induced-charge electrokinetic phenomena are actively investigated nowadays [14] due to potential applications in microfluidic pumping and mixing [15], particle manipulation [16], capacitive deionization [17], and control of ionic transport in nanochannels [18].

The ionic selectivity of a membrane can be characterized by the potential difference at zero current, which develops between two electrolyte solutions of different concentrations separated by the membrane [19,20]. In charged membranes, this difference arises due to Donnan equilibrium between the diffusion and electric forces at membrane-solution interfaces and the diffusion potential associated with different ionic mobilities [21]. The phenomenon of the membrane potential plays a fundamental role in the functioning of artificial and biological membranes [1–4].

In this Letter, we report a new mechanism for the generation of a membrane potential in polarizable nanoporous membranes. It occurs due to the induction of a surface charge by an electric field resulting from the diffusion of ions with different mobilities. It is shown theoretically and experimentally that this effect leads to a dramatic enhancement of the diffusion potential in uncharged polarizable membranes in comparison with their dielectric, nonpolarizable counterparts.

Theoretical model.—A membrane is modeled as an array of cylindrical pores of length L_p and radius R_p, which connect two reservoirs with the 1-1 electrolyte of concentrations C_L and C_R. The flow and ion transport are described by the space-charge model derived from Navier-Stokes, Nernst-Planck, and Poisson equations [22]. We introduce characteristic scales of radial R_p and axial L_p lengths, concentration $C_0 = 1$ mM, electric potential V_T, ion fluxes $D_- C_0/L_p$, velocity D_-/L_p, pressure $C_0 R_g T$, and surface charge density $\varepsilon\varepsilon_0 V_T/R_p$. Here $V_T = R_g T/F$ is the thermal voltage, $D_\pm$ are the cation and anion diffusion coefficients, and $\varepsilon\varepsilon_0$ is the dielectric constant. The dimensionless potential φ, ion concentrations $c_\pm$, and pressure p are written, respectively, as [22]

$$\varphi = \phi_v(z) + \psi(r,z), \qquad c_\pm = c_v(z)\exp[\mp\psi(r,z)],$$
$$p = p_v(z) + 2c_v(z)\cosh[\psi(r,z)].$$

The function ψ satisfies the Poisson equation

$$\frac{1}{r}\frac{\partial}{\partial r}\left(r\frac{\partial\psi}{\partial r}\right)=\frac{c_v(z)}{\lambda^2}\sinh\psi, \tag{1}$$

with boundary conditions $\partial\psi/\partial r(0,z)=0$ and

$$\psi(1,z)=\varphi_s-\phi_v(z) \quad \text{(const surface potential)} \tag{2}$$

$$\text{or} \quad \frac{\partial\psi}{\partial r}(1,z)=\sigma_s \quad \text{(const surface charge)}. \tag{3}$$

Here $\lambda=\sqrt{\varepsilon\varepsilon_0 V_T/2FC_0}/R_p$ is the dimensionless Debye length. The virtual variables ϕ_v, c_v, and p_v are found by solving the ordinary differential equation system

$$\left(\frac{dp_v}{dz},\frac{1}{c_v}\frac{dc_v}{dz},\frac{d\phi_v}{dz}\right)^T=L(\bar v,\bar j,\bar i)^T, \tag{4}$$

where $\bar v$ is the volume flux (velocity), $\bar j=\bar j_+ +\bar j_-$ is the ion flux, and $\bar i=\bar j_+ -\bar j_-$ is the ionic current (all fluxes are dimensionless and cross-sectionally averaged), while L is the symmetric 3×3 matrix, which coefficients $L_{ij}(z)$ are calculated using the solution $\psi(r,z)$; see Supplemental Material [23]. The membrane potential is measured at zero current $\bar i=0$ and equal pressures in both reservoirs. In this case, system (4) becomes

$$\begin{aligned}\frac{dp_v}{dz}&=L_{11}\bar v+L_{12}\bar j,\\ \frac{1}{c_v}\frac{dc_v}{dz}&=L_{12}\bar v+L_{22}\bar j,\\ \frac{d\phi_v}{dz}&=L_{13}\bar v+L_{23}\bar j.\end{aligned} \tag{5}$$

The corresponding boundary conditions are

$$\begin{aligned}z=0:&\quad p_v=-2c_L,\quad c_v=c_L,\quad \phi_v=0,\\ z=1:&\quad p_v=-2c_R,\quad c_v=c_R,\quad \phi_v=\Delta\varphi,\end{aligned} \tag{6}$$

where $\Delta\varphi$ is the dimensionless potential difference between the reservoirs (membrane potential).

We assume that the conductive nanopore wall is ideally polarizable and there is no charge exchange between the wall and electrolyte. The polarization by the electric field developing inside the pore causes the redistribution of the surface charge. In this case, the floating boundary condition should be used [18]:

$$\int_0^1\frac{\partial\psi}{\partial r}(1,z)dz=\bar\sigma_s. \tag{7}$$

Here $\bar\sigma_s=\bar\sigma(\varepsilon\varepsilon_0 V_T/R_p)^{-1}$ is the dimensionless total surface charge density, while the dimensional total surface charge is given by $\bar\sigma 2\pi R_p L_p$.

To the best of our knowledge, this is the first attempt of extending the classical space-charge model with a constant surface charge to nanopores with polarizable walls. The use of boundary condition (2) and integral condition (7) introduces some difficulties. The surface potential φ_s is not known in advance. The virtual potential $\phi_v(z)$ is found by the integration of system (5) with coefficients $L_{ij}(z)$, which in turn depend on the solution $\psi(r,z)$ of problem (1) and (2). It makes the system strongly coupled and nonlinear.

Let us express $dz=dc_v[c_v(L_{12}\bar v+L_{22}\bar j)]^{-1}$ from the second equation in (5) and substitute it into the first and third equations. Integration of the resulting equations (5) over the pore length with the help of boundary conditions (6) gives

$$\int_{c_L}^{c_R}\frac{L_{11}\bar f+L_{12}}{c_v(L_{12}\bar f+L_{22})}dc_v+2(c_R-c_L)=0, \tag{8}$$

$$\bar j=\int_{c_L}^{c_R}\frac{dc_v}{c_v(L_{12}\bar f+L_{22})}, \tag{9}$$

$$\phi_v(c_v)=\int_{c_L}^{c_v}\frac{L_{13}\bar f+L_{23}}{c_v(L_{12}\bar f+L_{22})}dc_v, \tag{10}$$

where $\bar f=\bar v/\bar j$. It follows from (1), (2), and (10) that one can write $\psi=\psi(r,c_v)$, $\phi_v=\phi(c_v)$, and $L_{ij}=L_{ij}(c_v)$; see also [22,23].

The calculation is performed as follows. For *a nonpolarizable dielectric nanopore* with constant surface charge density σ_s, problem (1) and (3) is solved numerically for a set of successive values $c_v=c_{vk}$, $k=0,\ldots,n$, where $c_{v0}=c_L$ and $c_{vn}=c_R$. Then the ratio of fluxes $\bar f=\bar v/\bar j$ is found numerically from (8), and the ion flux $\bar j$ is obtained from (9). The potential difference between reservoirs $\Delta\varphi=\phi_v(c_R)$ is determined from (10), while the virtual variables are found by integration of (5) and (6). For *a polarizable conductive nanopore* with constant total surface charge density $\bar\sigma_s$, the surface potential φ_s should be determined in order to satisfy the floating boundary condition (7). Here problem (1) and (2) is solved for each c_{vk} at fixed φ_s and $\bar f$. Note that $\phi_v(c_{v0})=\phi_v(c_L)=0$. The value $\phi_v(c_{vk})$ is found iteratively starting from $\phi_v(c_{v,k-1})$ and repeating the solution of (1) and (2) followed by the application of (10). The calculation is performed iteratively to find the fluxes ratio $\bar f$ from (8). Then $\bar j$ is calculated from (9), and virtual variables are obtained by the integration of (5) and (6). It allows us to find $\psi(r,z)=\psi(r,c_v(z))$ and finally calculate the integral in the left-hand side of (7). The whole procedure is iterated to find the surface potential φ_s, with which (7) is satisfied. Note that a numerical solution of Eq. (1) requires specifying $\psi(0,z)=\psi_0$ [23]. The initial approximation for ψ_0 is obtained analytically [24].

For a nonpolarizable and uncharged ($\sigma=0$) nanopore, the dimensional potential, concentrations, and pressure can be determined analytically [20]:

$$\Phi=V_T\frac{D-1}{D+1}\ln\frac{C_L}{C_\pm},\qquad C_\pm=C_L+\frac{C_R-C_L}{L}z, \tag{11}$$

and $P=0$. Here $D=D_+/D_-$ is the ratio of ion diffusion coefficients (or mobilities $u_\pm=D_\pm/V_T$). In this case, the membrane potential coincides with the diffusion potential:

$$\Delta\Phi = V_T \frac{D-1}{D+1} \ln \frac{C_L}{C_R}. \quad (12)$$

Membrane preparation and potential measurement.—To validate the predictions of the theoretical model experimentally, we have synthesized membranes with a dielectric as well as conductive nanoporous structure. The membranes are prepared from Nafen™ alumina nanofibers supplied by ANF Technologies (Estonia). The diameter of a single nanofiber is 10–15 nm, and the length is up to 100 mm. The nanofibers are dispersed in deionized water (the weight ratio of Nafen:water is 1:200) and agitated with a magnetic stirrer for 30 min followed by 15 min of ultrasonic treatment (Sonics & Materials VC-505, USA). The suspension is filtered through the rough Teflon filter (average pore size of 0.6 μm) to produce a membrane in the form of a circular disk with the diameter of ~40 mm and thickness of ~400 μm. The membrane is dried in air and sintered at 800 °C during 4 hr. Chemical vapor deposition is used to form conductive carbon layers on the nanofibrous membrane structure. The synthesis is conducted in a homemade reactor at 900 °C (heating rate of 20–30 °C/min) in a propane-nitrogen mixture (1/15) with the total flow rate of 4000 cm^3/min during 60 s. The samples with and without deposited carbon will be referred to as the C-Nafen membrane and the Nafen membrane, respectively. The dielectric Nafen membrane is characterized by the porosity of 75%, a specific surface area of 146 m^2/g, and a maximum of pore diameter distribution curve at 28 nm. The corresponding parameters of conductive C-Nafen membrane are 62%, 107 m^2/g, and 16 nm [25]. Both types of membranes are hydrophilic.

The membrane potential is measured in KCl and NaCl aqueous solutions in a laboratory-made electrochemical cell. The membrane is clamped between two half-cells with reference 4.2 M Ag/AgCl electrodes. The latter are connected to the potentiostat PI-50Pro (Elins, Russia), which measures the cell electromotive force. First, the solution with fixed concentration C_R is placed in both half-cells and kept at a room temperature of 25 °C during 12 hr. The measurements are performed by successively increasing the electrolyte concentration in the left half-cell. At each step, the system is allowed to equilibrate during 30 min before the measurement is made. More information about the membrane preparation and potential measurements can be found in Refs. [23,25].

Results and discussion.—The comparison between nonpolarizable and polarizable uncharged nanopores is shown in Fig. 1 for NaCl aqueous solution with $D_+ = 1.33 \times 10^{-9}$ and $D_- = 2.03 \times 10^{-9}$ m^2/s. In the former case described by Eq. (11), the concentrations of cations and anions coincide. The potential decrease results in the electric field $E = -\nabla\Phi$, which speeds up the slower diffusing cation and retards the faster diffusing anion to make the total ion fluxes equal. In a polarizable pore, this electric field induces the surface charge, which changes almost linearly from the pore entrance ($Z/L_p = 0$) to the pore exit ($Z/L_p = 1$) while keeping the total surface charge $\bar{\sigma}$ zero; see Fig. 1(d). It results in the higher concentration of cations (anions) at the negatively (positively) charged part of the pore [Fig. 1(b)]. The separation of charge induces the Donnan potentials at the pore entrance and exit, which both contribute to the enhancement of the membrane potential in comparison with the nonpolarizable pore [Fig. 1(a)]. It can be seen from Fig. 2(a) that the surface potential is constant (−2.7 mV), while the potential increases (decreases) in those regions of the pore where the concentration of cations (anions) is higher. The separation of charge also results in osmotic pressure jumps at the pore entrance and exit; see Fig. 1(c). They in turn induce the osmotic flow in the direction of higher salt concentration with the average velocity of 23 nm/s.

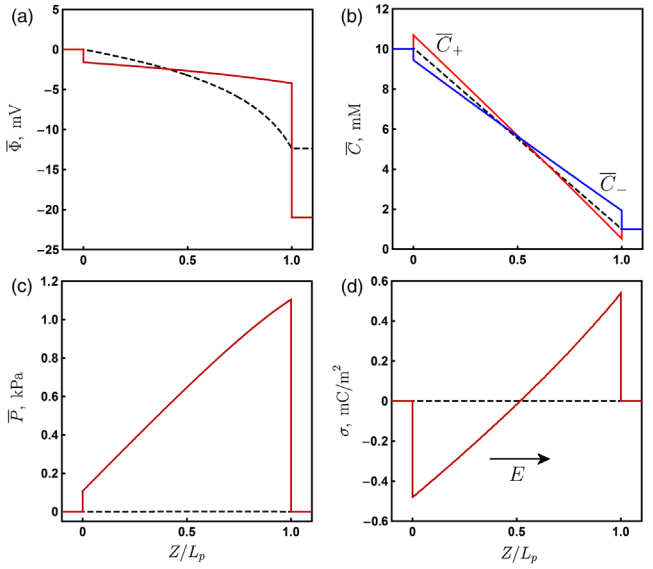

FIG. 1. The cross-sectionally averaged potential (a), concentrations (b), pressure (c), and surface charge density (d) for nonpolarizable ($\sigma = 0$, dashed curves) and polarizable ($\bar{\sigma} = 0$, solid curves) nanopores in NaCl solution. $R_p = 8$ nm, $L_p = 400$ μm, $C_L = 10$ mM, and $C_R = 1$ mM.

The calculated membrane potentials of uncharged nonpolarizable ($\sigma = 0$, $R_p = 14$ nm) and polarizable ($\bar{\sigma} = 0$, $R_p = 8$ nm) membranes in KCl and NaCl solutions are shown in Fig. 3 by dashed curves. The induced-charge

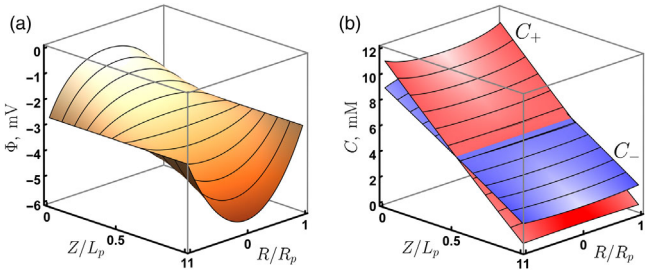

FIG. 2. The potential (a) and concentration (b) fields in a polarizable nanopore with $\bar{\sigma} = 0$ in NaCl solution (for parameters, see Fig. 1).

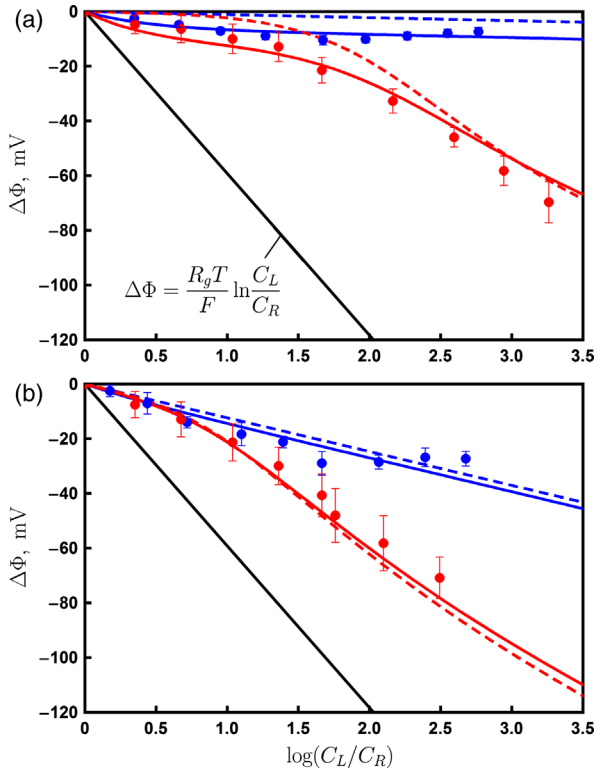

FIG. 3. Membrane potential of Nafen (blue lines) and C-Nafen (red lines) membranes in KCl (a) and NaCl (b) aqueous solutions. Experimental data (points), calculations for uncharged nonpolarizable (blue) and polarizable (red) pores (dashed curves), fitting of experimental data (solid curves), and ideal anion selectivity (solid black line). Error bars, 1 s.d.

enhancement of the diffusion potential for KCl solution with almost equal ion diffusion coefficients ($D_+ = 1.96 \times 10^{-9}$ m^2/s, $D_+/D_- = 0.96$) is quite significant [more than 16 times at $\log(C_L/C_R) = 3$]. For NaCl solution, the enhancement is around 2.6 times at the same concentration contrast, while the induced surface charge density varies in the range from -8.58 to 8.06 mC/m^2 along the pore [here the variation is much higher than that shown in Fig. 1(d)].

The theoretical results are well supported by the experimental data. The measurements for the Nafen membrane were performed near the point of zero charge for the alumina surface, which corresponds to $p\mathrm{H} = 9.1$ in KCl solution [26] and $p\mathrm{H} = 8.1$ in NaCl solution [27,28] (see also Supplemental Material [23]). The values of surface charge density σ obtained by fitting of the experimental data to the theoretical model of a nonpolarizable nanopore with $R_p = 14$ nm are presented in Table I. They are rather low, so the fitted curves only slightly deviate from those corresponding to $\sigma = 0$.

For a C-Nafen membrane with a conductive carbon surface, the adsorption of alkali metal cations on the defects of the carbon structure can occur and modify the surface charge [25,29]. To minimize this effect, low electrolyte concentrations were used: $C_R = 0.1$ mM for KCl and

TABLE I. Experimental cases with fitted values of σ (Nafen membranes) or R_p and $\bar{\sigma}$ (C-Nafen membranes).

Electrolyte	Aqueous KCl		Aqueous NaCl	
Membrane	Nafen	C-Nafen	Nafen	C-Nafen
C_R (mM)	1	0.1	1	1
R_p (nm)	14	8.8	14	9.4
σ or $\bar{\sigma}$ (mC/m^2)	0.329	0.039	0.128	0.045

$C_R = 1$ mM for NaCl. In this case, the experimental data were fitted to the theoretical model of the polarizable nanopore to obtain the total surface charge density $\bar{\sigma}$ and pore radius R_p; see Table I. The obtained values of $\bar{\sigma}$ are positive but rather small, while the R_p values are in good agreement with low-temperature nitrogen adsorption data (8 nm) [25]. So, the fitted curves are close to those of fully uncharged ($\bar{\sigma} = 0$) polarizable membranes in Fig. 3.

The diffusion potential of an uncharged nonpolarizable membrane depends only on the ratio of concentrations and ion diffusion coefficients; see Eq. (12). In the case of a membrane with polarizable pores, the situation is strikingly different. Figure 4(a) shows that the enhancement of the membrane potential becomes stronger with decreasing the concentration C_R. The calculations reveal that the variation of the averaged potential along the pore becomes smaller, while the Donnan potentials at the pore entrance and exit become larger when C_R decreases at fixed ratio C_L/C_R; see also Fig. 1. At smaller concentrations, the Debye length is

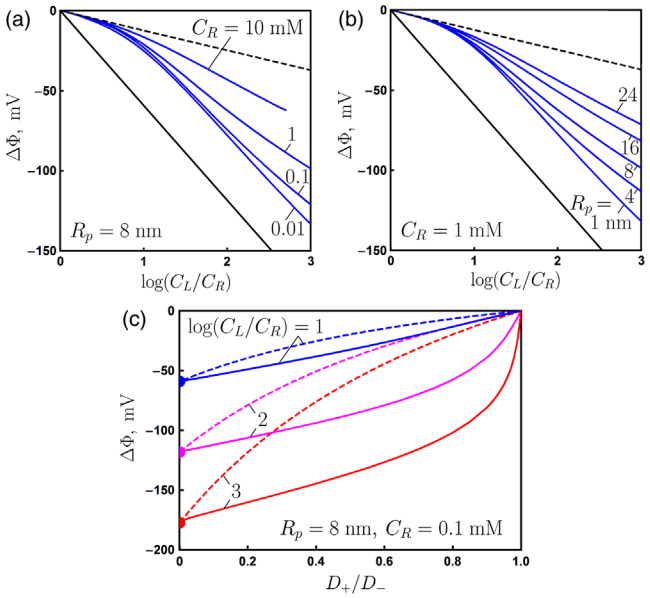

FIG. 4. The effect of concentration C_R (a) and pore radius R_p (b) on the membrane potential in NaCl aqueous solution for $\bar{\sigma} = 0$ (blue curves). Membrane potential for $\sigma = 0$ (dashed line) and ideal anion selectivity (solid black line). The effect of the diffusion coefficients ratio on the membrane potential (c) for uncharged nonpolarizable (dashed curves) and polarizable (solid curves) nanopores.

larger, which means a stronger overlap of electric double layers created by the induced surface charge. The same effect can be achieved by decreasing the pore radius; see Fig. 4(b). The membrane potential shows a significant increase when R_p decreases, but even at large R_p its enhancement is quite noticeable in comparison with the nonpolarizable case.

The effect of the ion diffusion coefficients ratio on the membrane potential is shown in Fig. 4(c). For both nonpolarizable and polarizable pores, $\Delta\Phi = 0$ when $D = D_+/D_- = 1$, while it approaches the Nernst potential when $D \to 0$; see Eq. (12). In the range $0 < D < 1$, a dramatic enhancement of the diffusion potential in a polarizable pore is observed. It becomes larger with increasing the concentration contrast. Especially unusual is the strong rise of the membrane potential magnitude near $D = 1$. It means that a very small difference between the diffusion coefficients can result in a large change of the membrane potential. This conclusion is confirmed by the experimental data in KCl solution; see Fig. 3(a). It can be shown from the model equations that, at the same ratio of smaller to larger diffusivity, the magnitude of the membrane potential is the same, but its sign is negative when $D_+ < D_-$ and positive when $D_+ > D_-$.

In summary, we have described a new mechanism for the generation of a membrane potential in polarizable nanoporous membranes. The electric field generated by the diffusion of ions with different mobilities induces a nonuniform surface charge, which results in a charge separation inside the nanopore. The corresponding Donnan potentials appear at the pore entrance and exit leading to a dramatic enhancement of the membrane potential in comparison with the uncharged dielectric membrane. The theoretical predictions are based on the space-charge model, which was extended to nanopores with a polarizable conductive surface. These predictions are confirmed experimentally by measuring the membrane potential in dielectric and conductive nanoporous membranes using KCl and NaCl aqueous solutions. The enhancement effect becomes greater with decreasing the electrolyte concentration and pore radius. A high sensitivity of the membrane potential to the ratio of ion diffusion coefficients is demonstrated. The described phenomenon may find applications in the precise determination of ion mobilities, electrochemical and biosensing, as well as the design of nanofluidic and bioelectronic devices.

This work is supported by the Russian Science Foundation, Project No. 15-19-10017.

*Corresponding author.
rii@icm.krasn.ru

[1] H. Strathmann, *Ion-Exchange Membrane Separation Processes* (Elsevier, Amsterdam, 2004).
[2] A. Cipollina and G. Micale, *Sustainable Energy from Salinity Gradients* (Elsevier/Woodhead Publishing, New York, 2016).
[3] F. G. Bănică, *Chemical Sensors and Biosensors: Fundamentals and Applications* (Wiley, Chichester, UK, 2012).
[4] J. Malmivuo and R. Plonsey, *Bioelectromagnetism—Principles and Applications of Bioelectric and Biomagnetic Fields* (Oxford University, New York, 1995).
[5] M. Tagliazucchi and I. Szleifer, Mater. Today **18**, 131 (2015).
[6] Z. S. Siwy and S. Howorka, Chem. Soc. Rev. **39**, 1115 (2010); X. Hou, W. Guo, and L. Jiang, Chem. Soc. Rev. **40**, 2385 (2011).
[7] W. Sparreboom, A. van den Berg, and J. C. T. Eijkel, Nat. Nanotechnol. **4**, 713 (2009); C. B. Picallo, S. Gravelle, L. Joly, E. Charlaix, and L. Bocquet, Phys. Rev. Lett. **111**, 244501 (2013).
[8] A. Siria, P. Poncharal, A. L. Biance, R. Fulcrand, X. Blase, S. T. Purcell, and L. Bocquer, Nature (London) **494**, 455 (2013).
[9] J. Bobacka, A. Ivaska, and A. Lewenstam, Chem. Rev. **108**, 329 (2008).
[10] Z. Siwy, I. D. Kosińska, A. Fuliński, and C. R. Martin, Phys. Rev. Lett. **94**, 048102 (2005).
[11] C. Lee, C. Cottin–Bizonne, A. L. Biance, P. Joseph, L. Bocquet, and C. Ybert, Phys. Rev. Lett. **112**, 244501 (2014).
[12] M. Nishizawa, V. P. Menon, and C. R. Martin, Science **268**, 700 (1995); C. R. Martin, M. Nishizawa, K. Jirage, M. Kang, and S. B. Lee, Adv. Mater. **13**, 1351 (2001).
[13] C. Yang, P. Hinkle, J. Menestrina, I. V. Vlassiouk, and Z. S. Siwy, J. Phys. Chem. Lett. **7**, 4152 (2016).
[14] M. Z. Bazant and T. M. Squires, Curr. Opin. Colloid Interface Sci. **15**, 203 (2010).
[15] M. Z. Bazant and T. M. Squires, Phys. Rev. Lett. **92**, 066101 (2004).
[16] S. Gangwal, O. J. Cayre, M. Z. Bazant, and O. D. Velev, Phys. Rev. Lett. **100**, 058302 (2008).
[17] S. Rubin, M. E. Suss, P. M. Biesheuvel, and M. Bercovici, Phys. Rev. Lett. **117**, 234502 (2016).
[18] C. Zhao, Y. Song, and C. Yang, Phys. Fluids **27**, 012003 (2015).
[19] P. Fievet, B. Aoubiza, A. Szymczyk, and J. Pagetti, J. Membr. Sci. **160**, 267 (1999).
[20] A. H. Galama, J. W. Post, H. V. M. Hamelers, V. V. Nikonenko, and P. M. Biesheuvel, J. Membr. Sci. Res. **2**, 128 (2016).
[21] Y. Tanaka, *Ion Exchange Membranes: Fundamentals and Applications* (Elsevier, Amsterdam, 2015).
[22] P. B. Peters, R. van Roij, M. Z. Bazant, and P. M. Biesheuvel, Phys. Rev. E **93**, 053108 (2016).
[23] See Supplemental Material at http://link.aps.org/supplemental/10.1103/PhysRevLett.119.226001 for solution of model equations and membrane potential measurement.
[24] S. Levine, J. R. Marriott, G. Neale, and N. Epstein, J. Colloid Interface Sci. **52**, 136 (1975).
[25] V. S. Solodovnichenko, D. V. Lebedev, V. V. Bykanova, A. V. Shiverskiy, M. M. Simunin, V. A. Parfenov, and I. I. Ryzhkov, Adv. Eng. Mater. **19**, 1700244 (2017).
[26] M. Tschapek, C. Wasowski, and R. M. Torres Sanchez, J. Electroanal. Chem. **74**, 167 (1976).
[27] R. Sprycha, J. Colloid Interface Sci. **127**, 1 (1989).
[28] Z. Saunders, C. W. Noack, D. A. Dzombak, and G. V. Lowry, J. Nanopart. Res. **17**, 140 (2015).
[29] G. Mpourmpakis and G. Froudakis, J. Chem. Phys. **125**, 204707 (2006).